Modelling of the intralaminar matrix damage with friction effects of fabric reinforced polymers

Sylvain Treutenaere, Franck Lauro, Bruno Bennani, Tsukatada Matsumoto, Ernesto Mottola

Composites Part B 111 (2017) 60e73

Modelling of the intralaminar matrix damage with friction effects of fabric reinforced polymers

S. Treutenaere [a], F. Lauro [a, *], B. Bennani [a], T. Matsumoto [b], E. Mottola [b]

[a] LAMIH, UMR CNRS 8201, Université de Valenciennes et du Hainaut-Cambrésis, CISIT, Mont Houy, F59313 Valenciennes CEDEX 9, France
[b] Toyota Motor Europe, Hoge Wei 33-Technical Center, Zaventem 1930, Belgium

E-mail *address:* franck.lauro@univ-valenciennes.fr (F. Lauro).

ABSTRACT

Needed to simulate the behaviour of industrial components through finite element analysis, a continuum damage model formulation for fabric reinforced polymers is provided. Based on the Onera Damage Microstructure Model, it considers the influence of privileged direction of intralaminar matrix damage on the stiffness. In this work, the stored strains are considered as representative of the position of the crack lips. Thus, after calculation of the stresses applied to the crack lips, a friction law has been newly implemented in order to represent the hysteresis loops during cyclic loading. Moreover, the possibility of a shear locking, very common among the textile simulations for large shearing, is introduced with its effect on the matrix damage. The present model is applied to simulate various fabric preforms (woven or non-crimp) under cyclic in-plane shear. Because of similarities of the physical phenomena which occur in each investigated materials, the present model is able to represent a realistic behaviour for every pre-forms investigated.

Keywords:
Composite
Textile
Damage
Friction
Large strain

1. Introduction

In these last decades, the use of carbon fabric reinforced thermoplastics (CFRP) in the automotive industry increased very significantly. The high specific stiffness and strength, the great energy absorption as well as the reduced manufacturing cost of these materials widely encourage their diffusion.

Previously limited to small runs (premium vehicles, racing), last advances in highly productive manufacturing process lead to the use of CFRP for high volume automotive production. Therefore, the behaviour understanding and modelling of these materials become essential for their implementation into the design loop, needed for the deployment on mass-produced vehicles. This article is focused on the non-linear behaviour introduced by the intralaminar matrix damage. As a consequence, the reinforcement damage, the strain-rate dependency as well as the interlaminar matrix damage (so-called delamination) are not considered in the present study.

Although not considered in this paper, the modelling of these last phenomena are on-going research topics. The strain-rate sensitivity can be introduced through phenomenological models [25,62], spectral models [13,66] or functional formulations [29,49,68,72,75]. Energetic fibre failure criteria have been proposed by Hill [30] and Tsai and Wu [71], but by coupling the different failure mechanisms the prediction is highly enhanced [2,25,37,51,57,60,74]. The propagation of the reinforcement damage can be regulated through non-local models [7,33,56,69], limitation of the damage rate [3,42,43] or by means of a smeared crack formulation [16,17,24,59] Regarding the delamination, the cohesive laws for fibre reinforced polymers have been, and still are, widely studied [4,15,27,34,48,53,58]. Another solution is the formulation of layered theories and specific finite elements dedicated to the simulation of laminated materials [6,8–11,23,38,39,47,63,64,67].

However, even if they contribute to the global behaviour of a CFRP structure, they are limited in case of in-plane quasi-static loading. The material model in its complete form is made up modules dedicated for each physical phenomenon. In this paper, the focus is only given on the modelling of the intralaminar matrix damage.

The present model is established within the framework of the Continuum Damage Mechanics (CDM). It was first introduced by Kachanov [35] and Rabotnov [61] by considering the damage as a distributed defects through defining thermodynamic state variables. These variables are categorised as observable (or measurable) state variables – such as strains, stresses or temperature – or

DOI : 10.1016/j.compositesb.2016.12.019

internal state variables (not directly measurable) – such as damage.

Thereafter, Lemaitre [46] introduced the concept of *equivalence principle* which gave a physical interpretation of damage variables. This idea is based on the definition of an *effective stress tensor*. It may be interpreted as the stress leading to the same amount of deformation by replacing the damaged material by a hypothetical virgin one.

Originally set for isotropic materials, such as metals, the use of CDM for anisotropic and composite materials was introduced by Chaboche [18] and Ladeveze and LeDantec [43]. The damage variables are given in null-, second- or fourth-order tensor forms. In case of privileged damage directions, scalar variables are sufficient to well-described the crack influences on the material behaviour. On the other hand, when the damage direction depends on the loading direction second- or fourth-order tensor forms are used.

Besides, it is important to take into account the unilateral character of damage. The closure of the crack, given by the stress state applied to it, leads to the recovery (partial or total) of the initial stiffness of the material. This unilateral character may be easily introduced thanks to the use of the Macaulay brackets for the stress normal to the crack orientation [1,43]. However, it leads to an incorrect behaviour in case of multi-axial loading [19]. Two approaches were then proposed by Chaboche:

- The first one consists of closing the diagonal terms of the stiffness tensor [20]. As a result, the initial shear stiffness is not recovered. Physically this may be seen as crack closure with a perfect slippage of the lips.
- The second approaches [21] leads to the complete recovery of the initial stiffness. By comparison to the previous one, it may be seen as an infinite friction between crack lips. In order to do so, an additional internal variable, the stored strain, is added to the model. It may be seen as representative of the position of the lips at closure. By definition it ensures the continuity at closure, but leads to discontinuities at re-opening when closure and opening do not occur at same loading configuration.

After a given loading/unloading then followed by a relaxation, permanent strains are observed and are imputed to the presence of damage. It can be explained by a release of residual stresses inherent to the manufacturing process and because of different thermal dilatations between the constituents [65,66], but also by friction effects and microscopic plasticity of the matrix in the vicinity of the cracks [1,43,50]. Schieffer et al. [66] models these permanent strains by means of residual strains evolving linearly with damage, whereas Ladeveze and LeDantec [43], Abisset et al. [1], Maim et al. [50] use a plastic formulation.

Regarding the modelling of the frictional microcracks, various micromechanical studies have been proposed in last decades. Based on Kachanov [36], these models proposed by Gambarotta and Lagomarsino [26], Basista and Gross [12], Krajcinovic and Fanella [41], Sumarac and Krajcinovic [70] are stress-based formulated and most of them do not follow a thermodynamic approach which allow an easy connection with macroscopic models. An interesting approach is proposed by Andrieux et al. [5] to model two-dimensional frictional sliding micro-cracks in a strain-space which follows the thermodynamic approach. Various authors have extended this framework such as Halm and Dragon [28], Wrzesniak et al. [73], Zhu et al. [76], Pense et al. [55] through different homogenisation techniques. However these methods are extremely complex to be implemented and coupled with pre-existing material models.

Further works took interest in micromechanical considerations such as the diffuse matrix damage or the fibre/matrix decohesion. A crack density, based on the stress and an energy balance, is introduced to take into account the ply thickness on the kinetics of damage [44,45]. Huchette et al. [32] integrated this microscopic crack density in a viscoelastic formulation to provide the latter additional non-linearity.

Marcin [52] adapted and extended the micromechanics based CDM model proposed by Chaboche and Maire [21] to the fabric reinforced materials. While remaining within the mesoscopic scale, he introduced a coupling between in-plane loading and damage normal to the thickness direction.

For the present work, the constitutive relation derived from Marcin's formulation is recalled Section 2. An adaptation of the stored strains to take into account the friction mechanisms inside the composite materials is formulated. This formulation allows a simple and efficient coupling with the Onera Damage Model. Hence, these friction mechanisms are strongly linked to the damage evolution and the model is able to represent the hysteresis loop during cyclic loading. The possibility of a shear locking for textile preforms is then added to the model. This shear locking leads to a damage mechanism which is added to the previous formulation. Section 4 concerns the identification of the model parameters. Finally the model, and particularly the friction mechanisms, is validated through simulations of quasi-static cyclic in-plane shear tests.

2. Continuum matrix damage model

This work relies on a closed version of the *Onera Damage Model MicroStructure* (ODM_MS) proposed by Marcin [52]. Although the model has to describe the physical mechanisms, it is intended to be used in an industrial environment. Hence, the ODM_MS being based at the mesoscopic scale and formulated in the strain-space (ideal for an implementation for finite element analysis), it was well suited for basis of the complete material model.

The matrix damage modelling is based on the assumption that the preferred damage directions at the mesoscopic scale correspond to the directions of reinforcement. This assumption is confirmed by basic experimental observations on two different fabric preforms after an in-plane shear test (Fig. 1).

Moreover, this model is able to depict the effects of the crack closure on the recovery of the initial stiffness. For this purpose the internal variable so-called stored strain, representative of the position of crack lips at closing, is used. However, as depicted by Chaboche and Maire [21], the re-opening may lead to stress discontinuities that may be critical for the stability of finite element analysis. A further development was to introduce friction effects but was never followed up.

Yet, these friction mechanisms are fundamental for structural simulations with complex loading, notably in case of positive/negative shear switchover. Consequently, an efficient and Coulomb-based friction formulation is introduced in the present model and is described in Section 2.8 relative to the stored strains.

Another important improvement is the consideration of the shear locking which is specific to textile preforms. The effect of the shear locking on the damage kinetics are also considered and is given Section 2.9.

2.1. Finite strain framework

Given the strong anisotropic behaviour induced by the reinforcement of the fabric composite plies, it is essential that the formulation may be able to follow the directions of anisotropy for large displacements and moderate strains. As a result, the base (or undeformed) and the current (deformed) configurations of the material cannot be assumed identical. This hypothesis is the basis of the small displacement and small deformation theory, making it

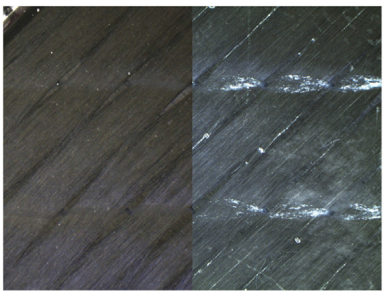

(a) Initial view of biaxial non-crimp fabric (left) and once damaged (right).

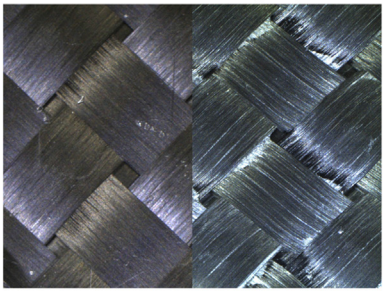

(b) Initial view of 3K plain-weave woven fabric (left) and once damaged (right).

Fig. 1. Global overview of cracks following an in-plane shear loading on various fabric reinforced polymers by observation of the external surface.

not applicable. Consequently, it is essential to extend the model in finite strain to ensure that the objectivity and the directions of anisotropy are well-assessed.

With few exceptions, Lagrangian (or Material) coordinates are used to describe the deformations of a solid. This approach facilitates the formulation of material constitutive models since the position and the physical properties of solid particles are described according to a reference position of these material particles and time. The choice of the reference configuration to express the strain and the stress quantities leads to strongly different formulations for the model.

Let $\mathrm{d}\overrightarrow{X}$ be a position vector which describes material points in the undeformed configuration. The material points in the deformed configurations are now described by $\mathrm{d}\overrightarrow{X}$. The change of the material points is defined by the function $x_i = m_i(X_I, t)$ which leads to the definition of the deformation gradient tensor $\underline{\mathbf{F}}$:

$$\mathrm{d}\overrightarrow{x} = \underline{\mathbf{F}}\cdot\mathrm{d}\overrightarrow{X} \quad \text{with} \quad F_{ij} = \frac{\partial x_i}{\partial X_J}. \tag{1}$$

From now, a distinction should be made between the tensors expressed according to the base configuration or the current configuration. In the total Lagrangian formulation, the reference is assumed to be the base configuration at each step of the iterative scheme used in finite element analysis.

The variation of the scalar product according to the material vectors in the base configuration is defined with:

$$\mathrm{d}\overrightarrow{x}\cdot\delta\overrightarrow{x} - \mathrm{d}\overrightarrow{X}\cdot\delta\overrightarrow{X} = 2\cdot\mathrm{d}\overrightarrow{X}\cdot\underline{\mathbf{E}}\cdot\delta\overrightarrow{X} \tag{2}$$

where $\underline{\mathbf{E}} = \frac{1}{2}(\underline{\mathbf{F}}^T\underline{\mathbf{F}} - \underline{\mathbf{I}})$ is called Green-Lagrange strain tensor.

Now, the stresses have to be evaluated according to the base configuration too. $\mathrm{d}\overrightarrow{f}$ is a force which acts on the current body and is the only one measurable from the experiments. Let $\mathrm{d}\overrightarrow{f}_0$ be a virtual force, seen as the equivalent of $\mathrm{d}\overrightarrow{f}$ which may act on the base configuration. $\mathrm{d}\overrightarrow{f}_0$ has no physical existence and is the transposition of $\mathrm{d}\overrightarrow{f}$ in the base configuration:

$$\mathrm{d}\overrightarrow{f}_0 = \underline{\mathbf{F}}^{-1}\mathrm{d}\overrightarrow{f}. \tag{3}$$

Hence, a stress tensor integrally based on the base configuration can be defined through the relation:

$$\mathrm{d}\overrightarrow{f}_0 = \underline{\mathbf{\Sigma}}\cdot\overrightarrow{N}\cdot\mathrm{d}S_0 \tag{4}$$

with $\underline{\mathbf{\Sigma}}$ the second Piola-Kirchhoff stress tensor (PK2) and $\underline{\mathbf{\Sigma}}$ is symmetric.

The incremental objectivity is ensured by the use of total Lagrangian tensors. Moreover, by referring all calculations on the base configuration, the directions of anisotropy are well-assessed throughout the shearing.

However, a problem potentially arises for large deformation by using a total Lagrangian formulation link to the scheme of the small deformation theory:

$$\underline{\boldsymbol{\sigma}} = \underline{\underline{\mathbf{C}}} : \underline{\boldsymbol{\varepsilon}} \Leftrightarrow \underline{\mathbf{\Sigma}} = \underline{\underline{\mathbf{C}}} : \underline{\mathbf{E}}. \tag{5}$$

In case of constant components for the stiffness tensor, a softening behaviour occurs for moderate compressive loading. To overcome this limitation, extended hyperelastic models based on invariants of strain tensors are developed [14,22,31,54]. But the present model is based on a model which is initially formulated by following the scheme of the small deformation. For obvious reasons of development time, the main body of the model given by the literature had to be kept. Accordingly the model validity is checked for the operating environment by verifying that the strain softening is not reached in compression. Because of the small deformations until failure in the fibre directions, this condition is respected.

A couple reasons ensure the possibility to simply extend the law which were formulated in small strains/small displacements to a total Lagrangian formulation. Firstly, the fabric reinforced plastics sustain moderate shear strains before failure. Obviously, the strain in the fibre directions raises no concern, knowing that the longitudinal strains remain small. Secondly, the problem arises for single shear strain of plies stacked in the same direction. De facto such

levels of shear will not, in practice, be reached as a result of multiaxial loading and of earlier failure.

2.2. Constitutive relation

The model is formulated in strain-space to ensure a good efficiency for FEA by using the Helmotz free energy as thermodynamic potential:

$$\psi = \frac{1}{2\rho}\left(\psi^{m} + \psi^{0} - \psi^{r} - \psi^{s}\right) \tag{6}$$

with

$$\begin{cases} \psi^{m} = \left(\underline{\mathbf{E}} - \underline{\mathbf{E}}^{0}\right) : \underline{\underline{\tilde{\mathbf{C}}}} : \left(\underline{\mathbf{E}} - \underline{\mathbf{E}}^{0}\right) \\ \psi^{0} = \left(\underline{\mathbf{E}} - \underline{\mathbf{E}}^{0}\right) : \underline{\underline{\mathbf{C}}}^{0} : \underline{\mathbf{E}}^{0} + \underline{\mathbf{E}}^{0} : \underline{\underline{\mathbf{C}}}^{0} : \left(\underline{\mathbf{E}} - \underline{\mathbf{E}}^{0}\right) \\ \psi^{r} = \left(\underline{\mathbf{E}} - \underline{\mathbf{E}}^{0}\right) : \underline{\underline{\mathbf{C}}}^{0} : \underline{\mathbf{E}}^{r} + \underline{\mathbf{E}}^{r} : \underline{\underline{\mathbf{C}}}^{0} : \left(\underline{\mathbf{E}} - \underline{\mathbf{E}}^{0}\right) \\ \psi^{s} = \left(\underline{\mathbf{E}} - \underline{\mathbf{E}}^{0}\right) : \underline{\underline{\mathbf{C}}}^{0} : \underline{\mathbf{E}}^{s} + \underline{\mathbf{E}}^{s} : \underline{\underline{\mathbf{C}}}^{0} : \left(\underline{\mathbf{E}} - \underline{\mathbf{E}}^{0}\right) \end{cases} \tag{7}$$

with the thermodynamic potentials ψ^{m} related to the matrix damage, ψ^{0} related to the initial state of the material, ψ^{r} related to the residual strains induced by microscopic plasticity of the matrix and ψ^{s} related to the stored strains representative of the position of the crack lips. Then the constitutive relation is obtained by derivation of this thermodynamic potential and is given by:

$$\underline{\mathbf{\Sigma}} = \rho\frac{\partial\psi}{\partial\underline{\mathbf{E}}} = \underline{\underline{\tilde{\mathbf{C}}}} : \left(\underline{\mathbf{E}} - \underline{\mathbf{E}}^{0}\right) - \underline{\underline{\mathbf{C}}}^{0} : \left(\underline{\mathbf{E}}^{r} + \underline{\mathbf{E}}^{s} - \underline{\mathbf{E}}^{0}\right). \tag{8}$$

$\underline{\mathbf{\Sigma}}$ and $\underline{\mathbf{E}}$ are respectively the second Piola-Kirchhoff stress tensor and the Green-Lagrange strain tensor (see Section 2.1). $\underline{\underline{\tilde{\mathbf{C}}}}$ and $\underline{\underline{\mathbf{C}}}^{0}$ are both fourth-order tensors which characterise the stiffness of the material. While $\underline{\underline{\mathbf{C}}}^{0}$ denotes the elastic stiffness tensor of the material, $\underline{\underline{\tilde{\mathbf{C}}}}$ represents the effective (damaged) stiffness tensor, evolving with the damage. $\underline{\mathbf{E}}^{0}$ represents the strain state where the cracks close off. It is due to the difference between the coefficients of thermal expansion of the matrix and of the reinforcement which creates residual stresses during the manufacturing. The residual strain $\underline{\mathbf{E}}^{r}$ and the stored strain $\underline{\mathbf{E}}^{s}$ are defined in Sections 2.6–2.8.

Thereafter, the Voigt notations are used to denote the second Piola-Kirchhoff stress tensor and the Green-Lagrange strain tensor. Both tensors are indeed symmetric and can be reduced to first-order tensors in order to simplify the establishment of the constitutive relation. Thus the previously mentioned second Piola-Kirchhoff stress tensor:

$$\underline{\mathbf{\Sigma}} = \begin{bmatrix} \Sigma_{11} & \Sigma_{12} & \Sigma_{13} \\ \Sigma_{21} & \Sigma_{22} & \Sigma_{23} \\ \Sigma_{31} & \Sigma_{32} & \Sigma_{33} \end{bmatrix} \tag{9}$$

can be reduced to the second Piola-Kirchhoff stress vector:

$$\begin{aligned} \vec{s} &= [\, s_1 \quad s_2 \quad s_3 \quad s_4 \quad s_5 \quad s_6 \,]^{T} \\ &= [\, \Sigma_{11} \quad \Sigma_{22} \quad \Sigma_{33} \quad \Sigma_{23} \quad \Sigma_{13} \quad \Sigma_{12} \,]^{T}. \end{aligned} \tag{10}$$

In the same way, the Green-Lagrange strain tensor:

$$\underline{\mathbf{E}} = \begin{bmatrix} E_{11} & E_{12} & E_{13} \\ E_{21} & E_{22} & E_{23} \\ E_{31} & E_{32} & E_{33} \end{bmatrix} \tag{11}$$

can be reduced to the Green-Lagrange strain vector:

$$\begin{aligned} \vec{e} &= [\, e_1 \quad e_2 \quad e_3 \quad e_4 \quad e_5 \quad e_6 \,]^{T} \\ &= [\, E_{11} \quad E_{22} \quad E_{33} \quad 2E_{23} \quad 2E_{13} \quad 2E_{12} \,]^{T}. \end{aligned} \tag{12}$$

Please note that $\vec{e}^{\,r}$, $\vec{e}^{\,s}$ and $\vec{e}^{\,0}$ are the respective Voigt notations of the strain Green-Lagrange tensors $\underline{\mathbf{E}}^{r}$, $\underline{\mathbf{E}}^{s}$ and $\underline{\mathbf{E}}^{0}$, and are determined in the same manner as $\vec{e}$ (Equation (12)). The shear components of $\vec{e}^{\,0}$ are considered null and the Green-Lagrange strain at crack closure is thus defined with Voigt notations by:

$$\vec{e}^{\,0} = \begin{bmatrix} e_1^{0} & e_2^{0} & e_3^{0} & 0 & 0 & 0 \end{bmatrix}^{T} \tag{13}$$

where e_i^{0} are parameters of the model.

Hence and by using the newly introduced stress and strain vectors, the constitutive relation can now be defined as follows:

$$\vec{s} = \underline{\underline{\tilde{\mathbf{C}}}} \cdot \vec{e} - \underline{\underline{\mathbf{C}}}^{0} \cdot \left(\vec{e}^{\,r} + \vec{e}^{\,s} - \vec{e}^{\,0}\right) \tag{14}$$

with

$$\vec{\tilde{e}} = \vec{e} - \vec{e}^{\,0}, \tag{15}$$

$\underline{\underline{\mathbf{C}}}^{0}$ the elastic second-order stiffness tensor and $\underline{\underline{\tilde{\mathbf{C}}}}$ the effective second-order stiffness tensor. $\underline{\underline{\mathbf{C}}}^{0}$ and $\underline{\underline{\tilde{\mathbf{C}}}}$ are respectively defined in Sections 2.3 and 2.4.

2.3. Elastic stiffness tensor

As a first step, the purely elastic behaviour of a fabric layer is described thanks to the elastic stiffness and compliance tensors, respectively $\underline{\underline{\mathbf{C}}}^{0}$ and $\underline{\underline{\mathbf{S}}}^{0} = (\underline{\underline{\mathbf{C}}}^{0})^{-1}$. In view of the architecture of the preforms with two orthogonal directions of reinforcement, the layers have orthotropic behaviours.

As a result in the material coordinate system of each preform previously defined, the compliance tensor takes the form:

$$\underline{\underline{\mathbf{S}}}^{0} = \begin{pmatrix} \frac{1}{E_1} & -\frac{\nu_{21}}{E_2} & -\frac{\nu_{31}}{E_3} & 0 & 0 & 0 \\ -\frac{\nu_{12}}{E_1} & \frac{1}{E_2} & -\frac{\nu_{32}}{E_3} & 0 & 0 & 0 \\ -\frac{\nu_{13}}{E_1} & -\frac{\nu_{23}}{E_2} & \frac{1}{E_3} & 0 & 0 & 0 \\ 0 & 0 & 0 & \frac{1}{G_{23}} & 0 & 0 \\ 0 & 0 & 0 & 0 & \frac{1}{G_{13}} & 0 \\ 0 & 0 & 0 & 0 & 0 & \frac{1}{G_{12}} \end{pmatrix}. \tag{16}$$

Among the twelve coefficients introduced in these last tensors, three groups can be distinguished:

- E_i, the elastic modulus along the axis i,
- G_{ij}, the shear modulus of a plane normal to the axis i in the direction j,
- and ν_{ij}, Poisson's ratios reflecting the deformation in direction j under imposed displacement in direction i.

Whereas the elastic shear modulus G_{ij} are considered constant, the elastic behaviour in the directions of reinforcement is non-linear. It is imputed to both yarn flattening and intrinsic non-linear elasticity of carbon fibres, explained by the rotation of

graphite crystallites toward the fibre direction [40]. The elastic modulus E_1 and E_2 are hence function of the strain by following the relations

$$E_i = E_i^0 + \alpha_i \cdot e_i, \quad i \in \{1,2\}. \tag{17}$$

where E_i^0 and α_i are material parameters.

Symmetry of stiffness and compliance tensors is used to reduce the number of parameters. The elastic behaviour can be fully described by nine independent elastic coefficients and three Poisson's ratios are arbitrarily taken to be dependent of the others. They are obtained from the relation:

$$\nu_{ij} = \nu_{ji} \cdot \frac{E_i}{E_j} \quad \text{with } i \in \{2,3\}, j \in \{1,2\} \text{ and } i \neq j. \tag{18}$$

2.4. Effective stiffness tensor

The damage is introduced by adding additional compliance to the elastic compliance tensor $\underline{\mathbf{S}}^0$, and as first step in the establishment of the model, only the matrix damage is considered. The effective compliance tensor is thus defined as $\underline{\tilde{\mathbf{C}}} = (\underline{\tilde{\mathbf{S}}})^{-1}$ with $\underline{\tilde{\mathbf{S}}} = \underline{\mathbf{S}}^0 + \underline{\Delta \mathbf{S}}^{\mathrm{m}}$. The additional compliance tensor due to the matrix damage is given by:

$$\underline{\Delta \mathbf{S}}^{\mathrm{m}} = \sum_i \eta_i^{\mathrm{m}} d_i^{\mathrm{m}} \underline{\mathbf{H}}_i^{\mathrm{m}} \tag{19}$$

where $\underline{\mathbf{H}}_i^{\mathrm{m}}$ is the compliance tensor associated with the damage variable d_i^{m}. This model uses three damage variables, two corresponding to the damage along the directions of reinforcement while the last one is used to describe the out-of-plane damage. η_i^{m} represents the crack closure index which varies from 0 (closed crack) to 1 (opened crack). It is defined by the following relation:

$$\eta_i^{\mathrm{m}} = \begin{cases} 1 & \text{if } \Delta e_i \leq \overline{e}_i \\ \frac{1}{2}\left(1 - \cos\left(\frac{\pi}{2}\,\frac{\overline{e}_i + \Delta e_i}{\Delta e_i}\right)\right) & \text{if } -\Delta e_i \leq \overline{e}_i \leq \Delta e_i \\ 0 & \text{if } \overline{e}_i \leq -\Delta e_i \end{cases}. \tag{20}$$

Δe_i depicts a strain tolerance between a state where all cracks are closed and a state where all cracks are open. This dispersion being closely tied to the number of cracks, Δe_i is set dependent to the crack ratio by the relation:

$$\Delta e_i = (1 + a_i^{\mathrm{m}} \cdot d_i^{\mathrm{m}}) \Delta e_i^0 \tag{21}$$

where a_i^{m} and Δe_i^0 are parameters of the model.

In order to describe separately the different fracture modes the compliance tensor $\underline{\mathbf{H}}_i^{\mathrm{m}}$ is split into both compliance tensors:

$$\underline{\mathbf{H}}_i^{\mathrm{m}} = \underline{\mathbf{H}}_i^{\mathrm{nm}} + \underline{\mathbf{H}}_i^{\mathrm{tm}}. \tag{22}$$

$\underline{\mathbf{H}}_i^{\mathrm{nm}}$ depicts the additional compliance due to normal loading to the crack (mode I) and $\underline{\mathbf{H}}_i^{\mathrm{tm}}$ the additional compliance due to tangent loading to the crack (mode II and III). They are defined by

$$\underline{\mathbf{H}}_1^{\mathrm{tm}} = \begin{pmatrix} h_{m(1)}^{\mathrm{I}} S_{11}^0 & 0 & 0 & 0 & 0 & 0 \\ 0 & 0 & 0 & 0 & 0 & 0 \\ 0 & 0 & 0 & 0 & 0 & 0 \\ 0 & 0 & 0 & 0 & 0 & 0 \\ 0 & 0 & 0 & 0 & 0 & 0 \\ 0 & 0 & 0 & 0 & 0 & 0 \end{pmatrix}, \tag{23}$$

$$\underline{\mathbf{H}}_1^{\mathrm{tm}} = \begin{pmatrix} h_{m(1)}^{\mathrm{I}} S_{11}^0 & 0 & 0 & 0 & 0 & 0 \\ 0 & 0 & 0 & 0 & 0 & 0 \\ 0 & 0 & 0 & 0 & 0 & 0 \\ 0 & 0 & 0 & 0 & 0 & 0 \\ 0 & 0 & 0 & 0 & h_{m(1)}^{\mathrm{III}} S_{55}^0 & 0 \\ 0 & 0 & 0 & 0 & 0 & h_{m(1)}^{\mathrm{II}} S_{66}^0 \end{pmatrix} \tag{24}$$

and $\underline{\mathbf{H}}_2^{\mathrm{nm}}, \underline{\mathbf{H}}_3^{\mathrm{nm}}, \underline{\mathbf{H}}_2^{\mathrm{tm}}$ and $\underline{\mathbf{H}}_3^{\mathrm{tm}}$ are obtained by index permutations. $h_{m(i)}^{\mathrm{I}}, h_{m(i)}^{\mathrm{II}}$ and $h_{m(i)}^{\mathrm{III}}$ are parameters of the model.

2.5. Damage evolution

By following the same approach than the additional compliance tensor, two driving forces affect the evolution of each damage variable: the normal y_i^{nm} and the tangential y_i^{tm} to the damage directions and are defined by

$$\begin{cases} y_1^{\mathrm{nm}} = \frac{1}{2} e_1^+ C_{11}^0 e_1^+ \\ y_1^{\mathrm{tm}} = \frac{1}{2}\left(e_4^+ C_{44}^0 e_4^+ + b_1 e_6^+ C_{66}^0 e_6^+\right) \end{cases} \tag{25}$$

where $y_2^{\mathrm{nm}}, y_3^{\mathrm{nm}}, y_2^{\mathrm{tm}}$ and y_3^{tm} are obtained by index permutations and b_1, b_2 and b_3 are material parameters. The thermodynamic forces so defined are dependent of the effective strain tensor $\underline{\mathbf{E}}^+$, which corresponds to the positive part of the spectral decomposition:

$$\underline{\mathbf{E}}^+ = \underline{\mathbf{P}} \cdot \begin{pmatrix} \langle E_{\mathrm{I}} \rangle & 0 & 0 \\ 0 & \langle E_{\mathrm{II}} \rangle & 0 \\ 0 & 0 & \langle E_{\mathrm{III}} \rangle \end{pmatrix} \cdot \underline{\mathbf{P}}^T \tag{26}$$

where $E_{\mathrm{I}}, E_{\mathrm{II}}$ and E_{III} are the eigenvalues of $\underline{\mathbf{E}}$ and $\underline{\mathbf{P}}$ the transformation matrix formed by the eigenvectors. Lastly e_i^+ are the components of $\overline{e}^{+}$, namely the Voigt notation of $\underline{\mathbf{E}}^+$.

From these thermodynamic forces the damage criterion is defined as follows:

$$F_i^{\mathrm{m}} = f_i^{\mathrm{nm}}(y_i^{\mathrm{nm}}) + f_i^{\mathrm{tm}}(y_i^{\mathrm{tm}}) - d_i^{\mathrm{m}} \leq 0 \tag{27}$$

with f the cumulative distribution function of Weibull:

$$f_i^{\mathrm{x}} = d_{c(i)}^{\mathrm{x}} \cdot \left[1 - \exp\left(-\left(\frac{\left\langle \sqrt{y_i^{\mathrm{x}}} - \sqrt{y_{0(i)}^{\mathrm{x}}} \right\rangle}{\sqrt{y_{c(i)}^{\mathrm{x}}}}\right)^{p_i^{\mathrm{x}}}\right)\right] \tag{28}$$

where $d_{c(i)}^{\mathrm{x}}, y_{0(i)}^{\mathrm{x}}, y_{c(i)}^{\mathrm{x}}$ and p_i^{x} are material parameters with "x" taking the value "nm" or "tm".

2.6. Residual strain

Following the appearance of damage, the strains do not recover potentially their initial state when the stresses are relaxed. Some phenomena close to the cracks and which occur at a microscopic scale such as micro-plasticity or debris inside gaps may prevent a

complete closure.

Following the description given by Marcin [52] for the ODM_MS, the residual strains are determined by following the relation:

$$\dot{\vec{e}}^{\,\mathrm{r}} = \underline{\mathbf{S}}^0 \cdot \left(\sum_i \zeta_i \eta_i^{\mathrm{m}} \dot{d}_i^{\mathrm{m}} \underline{\tilde{\mathbf{C}}} \cdot \underline{\mathbf{H}}_i^{\mathrm{m}} \cdot \underline{\tilde{\mathbf{C}}} \right) \cdot \vec{e} \tag{29}$$

where ζ_i is a parameter of the model.

However, for further developments dedicated to extend the formulation of the stored strains (Section 2.8), the evolution of the residual strains has to be split according to each crack direction and into two components. The first one corresponds to the evolution due to opening following a mode I (normal loading) of the cracks normal to the direction i, mentioned as $\dot{\vec{e}}_i^{\,\mathrm{r,nm}}$, while the second one corresponds to the opening following a mode II or III (tangential loading) of the cracks normal to the direction i, mentioned as $\dot{\vec{e}}_i^{\,\mathrm{r,tm}}$. They are determined by the following relations:

$$\dot{\vec{e}}_i^{\,\mathrm{r,nm}} = \underline{\mathbf{S}}^0 \cdot \left(\zeta_i \eta_i^{\mathrm{m}} \dot{d}_i^{\mathrm{m}} \underline{\tilde{\mathbf{C}}} \cdot \underline{\mathbf{H}}_i^{\mathrm{nm}} \cdot \underline{\tilde{\mathbf{C}}} \right) \cdot \vec{e}, \tag{30}$$

$$\dot{\vec{e}}_i^{\,\mathrm{r,tm}} = \underline{\mathbf{S}}^0 \cdot \left(\zeta_i \eta_i^{\mathrm{m}} \dot{d}_i^{\mathrm{m}} \underline{\tilde{\mathbf{C}}} \cdot \underline{\mathbf{H}}_i^{\mathrm{tm}} \cdot \underline{\tilde{\mathbf{C}}} \right) \cdot \vec{e}, \tag{31}$$

and the total evolution of the residual strains are then recovered by:

$$\dot{\vec{e}}^{\,\mathrm{r}} = \sum_i \left(\dot{\vec{e}}_i^{\,\mathrm{r,nm}} + \dot{\vec{e}}_i^{\,\mathrm{r,tm}} \right). \tag{32}$$

2.7. Stored strain

By contrast with the residual strain formulation, the evolution of the stored strains do not depend on the evolution of the damage ($\dot{d}_i^{\mathrm{m}}$) but on the evolution of the crack closure index ($\dot{\eta}_i^{\mathrm{m}}$). It is given by the relation:

$$\dot{\vec{e}}^{\,\mathrm{s}} = -\underline{\mathbf{S}}^0 \cdot \left(\sum_i \dot{\eta}_i^{\mathrm{m}} d_i^{\mathrm{m}} \underline{\tilde{\mathbf{C}}} \cdot \underline{\mathbf{H}}_i^{\mathrm{m}} \cdot \underline{\tilde{\mathbf{C}}} \right) \cdot \vec{e}. \tag{33}$$

The stored strain was initially introduced by Chaboche and Maire [21] to ensure the recovery of the initial elastic stiffness after the damage deactivation. Moreover, it avoids as well a discontinuity of the $(\vec{s}, \vec{e})$ response for complex loading cases. To illustrate the effect of the stored strains, an example of complex loading case, which consists of cyclic simple shear and traction/compression, is applied to a single shell element (Fig. 2).

By looking at the stress response of the model, it appears that the implementation of the stored strains ensures the continuity of the shear stress in case of opening or closure of the cracks (Fig. 3).

2.8. Introduction of friction mechanisms

Physically, the stored strain $\vec{e}^{\,\mathrm{s}}$ can be regarded as representative of the position of the crack lips after closure. For this above formulation, the hypothesis of infinite friction coefficient for closed crack (no evolution of the stored strain after the crack closure) makes the model unable to describe a realistic shear behaviour. To further improve the matrix damage model, an original and minimalist way to introduce friction effects at crack lips is presented in the rest of this section.

First, it is convenient to temporary rewrite the constitutive equation (14):

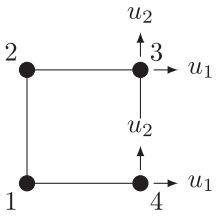

(a) Shell element used for tests on stored strains.

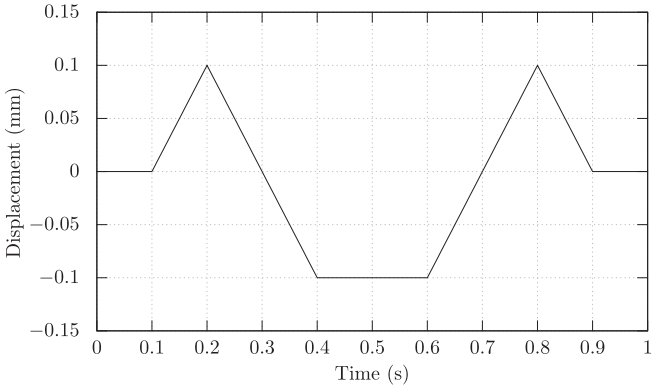

(b) u_1 displacement of nodes 3 & 4

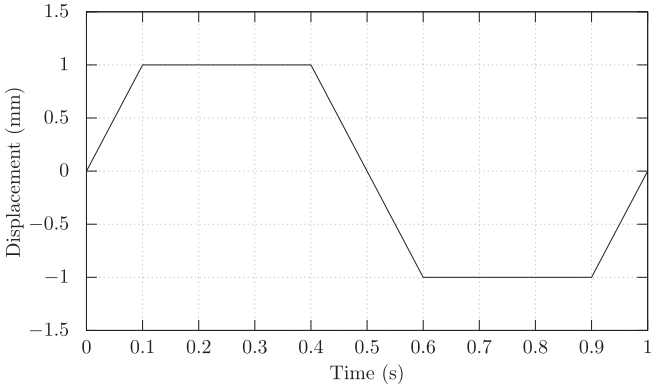

(c) u_2 displacement of nodes 3 & 4

Fig. 2. Imposed complex displacements for visualisation of the stored strain effect.

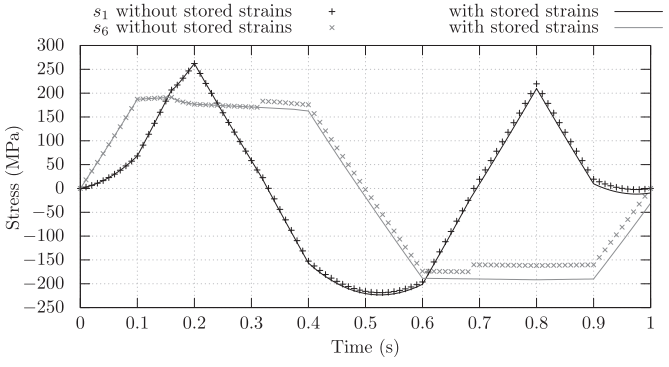

Fig. 3. Visualisation of the stored strain effect on the continuity of the stress response.

$$\vec{s} = \vec{s}^{\,\mathrm{e}} + \vec{s}^{\,\mathrm{m}} \tag{34}$$

where

$$\overrightarrow{s}^{e} = \left(\underline{\mathbf{S}}^{0} + \sum_{i} d_i^{m}\underline{\mathbf{H}}_i^{m}\right)^{-1} \cdot \overrightarrow{\overline{e}} \tag{35}$$

is the stress applied on the healthy zone of a representative volume element, and

$$\overrightarrow{s}^{m} = \underline{\mathbf{C}}^{0} \cdot \overrightarrow{e}^{0} + \sum_{i}\left[(1-\eta_i^{m}) d_i^{m}\tilde{\underline{\mathbf{C}}} \cdot \underline{\mathbf{H}}_i^{m} \cdot \underline{\mathbf{C}}^{0} \cdot \overrightarrow{\overline{e}} - \underline{\mathbf{C}}^{0} \cdot \left(\overrightarrow{e}_i^{r} + \overrightarrow{e}_i^{s}\right)\right] \tag{36}$$

is the stress applied on an area which surrounds the closed cracks normal to the i-direction (Fig. 4). Note that the open cracks are not considered in this constitutive relation since an open crack is unable to carry loads.

Then, to further apply a Coulomb friction law for the cracks, the normal and the tangential stresses, respectively $\overrightarrow{s}_i^{nm}$ and $\overrightarrow{s}_i^{tm}$, which act on the closed cracks are isolated. They are then given by:

$$\overrightarrow{s}_i^{nm} = (1-\eta_i^{m}) d_i^{m}\tilde{\underline{\mathbf{C}}} \cdot \underline{\mathbf{H}}_i^{nm} \cdot \underline{\mathbf{C}}^{0} \cdot \overrightarrow{\overline{e}} - \underline{\mathbf{C}}^{0} \cdot \left(\overrightarrow{e}_i^{r,nm} + \overrightarrow{e}_i^{s,nm} - \overrightarrow{e}_i^{0,nm}\right) \tag{37}$$

with $e_{ij}^{0,nm} = \delta_{ij} \cdot e_j^{0}$ where δ_{ij} is the Kronecker symbol, and

$$\overrightarrow{s}_i^{tm} = (1-\eta_i^{m}) d_i^{m}\tilde{\underline{\mathbf{C}}} \cdot \underline{\mathbf{H}}_i^{tm} \cdot \underline{\mathbf{C}}^{0} \cdot \overrightarrow{\overline{e}} - \underline{\mathbf{C}}^{0} \cdot \left(\overrightarrow{e}_i^{r,tm} + \overrightarrow{e}_i^{s,tm}\right). \tag{38}$$

As a result, a criterion which states that the cracks are subject to static friction ($\leq$0) or to dynamic friction (>0) is introduced and is given by:

$$\overline{s}_i^{s} = \left\|\overrightarrow{s}_i^{tm}\right\| - \mu_i \left\|\overrightarrow{s}_i^{nm}\right\|. \tag{39}$$

where μ_i is a coefficient of friction.

In case of a positive friction criterion, the crack lips start sliding to recover an equilibrium state. In the present work, the simplest modelling of the friction effect is considered, and is based on two hypotheses:

- the dynamic friction coefficient is equal to the static friction coefficient μ_i, thus the equilibrium state is recovered when the friction criterion $\overline{s}_i^{s}$ is null again;
- and the displacement of the lips, to recover the equilibrium state, is instantaneous.

It leads to the following equation:

$$\overline{s}_i^{s} + \Delta\overline{s}_i^{s} = 0, \tag{40}$$

with $\Delta\overline{s}_i^{s}$ the instantaneous evolution of the friction criterion to recover an equilibrium state. Since the normal stress applied to a crack does not evolve during sliding, the instantaneous evolution of the friction criterion is equal to the norm of the variation of the tangential stress applied to the crack:

$$\Delta\overline{s}_i^{s} = \left\|\Delta\overrightarrow{s}_i^{tm}\right\|. \tag{41}$$

Thus it is now possible to determine $\Delta\overrightarrow{s}_i^{tm}$, the vector notation of the variation of the tangential stress applied to the crack, by following the relation:

$$\Delta\overrightarrow{s}_i^{tm} = -\overline{s}_i^{s} \cdot \frac{\overrightarrow{s}_i^{tm}}{\left\|\overrightarrow{s}_i^{tm}\right\|}. \tag{42}$$

Finally, as $\Delta\overrightarrow{s}_i^{tm}$ is only dependent on the tangential displacement of the crack lips and by using equation (38), the evolution of the tangential stored strains due to the friction mechanisms are determined by using the following equation:

$$\Delta\overrightarrow{e}_i^{s,tm} = -\underline{\mathbf{S}}^{0} \cdot \Delta\overrightarrow{s}_i^{tm}. \tag{43}$$

However from a microscopic aspect the friction coefficient is dependent on the roughness of the crack lips. And there is definitely no one unique condition of surface, which leads to introduce a dispersion on the friction. Instead of considering all closed cracks together, N families are introduced and the stress applied to the closed cracks is assumed to be homogeneously distributed on them. Thus, for a family j of cracks normal to the i-direction, the normal and the tangential stress, respectively $\overrightarrow{s}_{ij}^{nm}$ and $\overrightarrow{s}_{ij}^{tm}$, are given by:

$$\overrightarrow{s}_{ij}^{nm} = (1-\eta_i^{m}) d_i^{m}\tilde{\underline{\mathbf{C}}} \cdot \underline{\mathbf{H}}_i^{nm} \cdot \underline{\mathbf{C}}^{0} \cdot \overrightarrow{\overline{e}} - \underline{\mathbf{C}}^{0} \cdot \left(\overrightarrow{e}_i^{r,nm} + \overrightarrow{e}_{ij}^{s,nm} - \overrightarrow{e}_i^{0,nm}\right) \tag{44}$$

and

$$\overrightarrow{s}_{ij}^{tm} = (1-\eta_i^{m}) d_i^{m}\tilde{\underline{\mathbf{C}}} \cdot \underline{\mathbf{H}}_i^{tm} \cdot \underline{\mathbf{C}}^{0} \cdot \overrightarrow{\overline{e}} - \underline{\mathbf{C}}^{0} \cdot \left(\overrightarrow{e}_i^{r,tm} + \overrightarrow{e}_{ij}^{s,tm}\right). \tag{45}$$

Then, the evolution of the tangential stored strains $\Delta\overrightarrow{e}_{ij}^{s,tm}$ is determined by following the procedure given by equations (39)–(43). The only difference is the use of a coefficient of friction μ_{ij} proper to each group. Finally the total stored strain evolution due to friction mechanisms is obtained by averaging every movements of crack lips:

$$\Delta\overrightarrow{e}_i^{s,tm} = \frac{1}{N}\sum_{j=1}^{N}\Delta\overrightarrow{e}_{ij}^{s,tm}. \tag{46}$$

About the range of the coefficients of friction, a quadratic and homogeneous distribution on a given interval is carried out. Thus they are computed by following the relation:

$$\mu_{ij} = \frac{\mu_i^{max}}{N^2} \cdot j^2 \quad \text{with } j \in [0, N-1]. \tag{47}$$

However, as for the crack closure index, the distribution of the friction coefficients is sensitive to the damage. As a result the upper bound of their range is given by:

$$\mu_i^{max} = (1 + m_i^{m} \cdot d_i^{m})\mu_i^{0} \tag{48}$$

where m_i^{m} and μ_i^{0} are parameters of the model.

2.9. Particularities of the textile preforms

In the particular case of plies made up with textile preforms – where the yarns are interlaced – the shear locking phenomenon occurs when the adjacent yarns come into contact. It results a

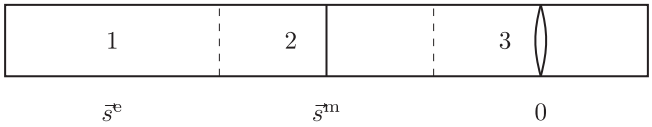

Fig. 4. Representative Volume Element and corresponding transmitted stresses of the area 1 (an healthy area), the area 2 (where the crack are closed) and the area 3 (where the cracks are open).

significant and progressive rise in the in-plane shear stiffness. In this model, the shear locking is introduced by using the following relation:

$$G_{12} = G_{12}^0 + g_{12}^{\mathrm{l}} \cdot \left\langle e_6 - e_6^{\mathrm{l}} \right\rangle \tag{49}$$

where $G_{12}^0, g_{12}^{\mathrm{l}}$ and e_6^{l} are parameters of the model. Note that the operator $\langle \cdot \rangle$ is called the Macauley bracket and $\langle x \rangle = x$ if $x > 0$, and null in others cases.

Also, it has been proved that the large shearing ability of the textile plies leads to massive out-of plane damages even for purely in-plane loading (Fig. 5). Its emergence is due to the opposite directions of rotation of transverse yarns. As a result, the matrix between both transverse yarns in the crossing area is subjected to torsion and causes breaking.

Marcin [52] introduced an in-plane/out-of-plane coupling by using a new thermodynamic force characterising these torsional modes. Consequently, the out-of plane damage is controlled by the previously defined normal and tangential forces, and the newly introducing coupling force:

$$\begin{cases} y_3^{\mathrm{nm}} = \dfrac{1}{2} e_3^+ C_{33}^0 e_3^+ \\ y_3^{\mathrm{tm}} = \dfrac{1}{2} \left(e_4^+ C_{44}^0 e_4^+ + b_3 e_5^+ C_{55}^0 e_5^+ \right) \\ y_3^{\mathrm{p}} = \dfrac{1}{2} e_6^+ C_{66}^0 e_6^+ \end{cases} . \tag{50}$$

The associated damage criterion is then actualised and given by:

$$F_3^{\mathrm{m}} = f_3^{\mathrm{nm}}(y_3^{\mathrm{nm}}) + f_3^{\mathrm{tm}}(y_3^{\mathrm{nm}}) + f_3^{\mathrm{p}}(y_3^{\mathrm{p}}) - d_3^{\mathrm{m}} \leq 0. \tag{51}$$

But in addition to Marcin's formulation, the in-plane shear stiffness is considered sensitive to the out-of-plane damage since the rotation between both transverse yarns is made easier. Thus, the additional compliance tensor due to tangential loading is modified to take into account this influence and is now given by:

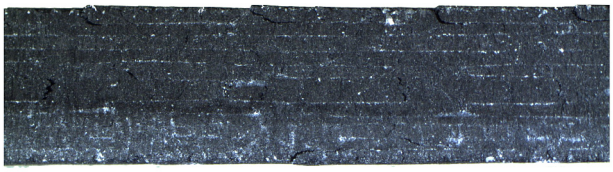

(a) Biaxial non-crimp fabric

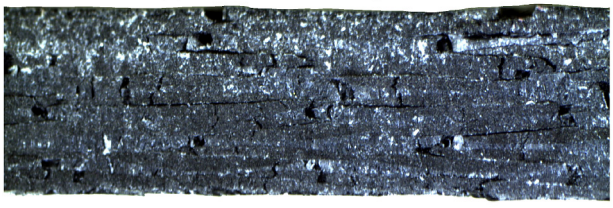

(b) 3K plain-weave woven

Fig. 5. Global overview of cracks following an in-plane shear loading on various fabric reinforced polymers by observation of the cross-section.

$$\underline{\mathbf{H}}_3^{\mathrm{tm}} = \begin{pmatrix} 0 & 0 & 0 & 0 & 0 & 0 \\ 0 & 0 & 0 & 0 & 0 & 0 \\ 0 & 0 & 0 & 0 & 0 & 0 \\ 0 & 0 & 0 & h_{m(3)}^{\mathrm{II}} S_{44}^0 & 0 & 0 \\ 0 & 0 & 0 & 0 & h_{m(3)}^{\mathrm{III}} S_{55}^0 & 0 \\ 0 & 0 & 0 & 0 & 0 & h_{m(3)}^{\mathrm{p}} S_{66}^0 \end{pmatrix} . \tag{52}$$

Therefore, the matrix damage model is able to consider a loss of the elastic stiffness and to take into account an eventual local plasticity around the cracks, the friction mechanisms and the shear locking of the textile preforms. Regarding the friction, the coefficients are evolving with the damage value.

2.10. Verification of the thermodynamic consistency

As a result of the addition of the friction mechanisms inside the material model, the consistency with regards to the thermodynamic laws needs to be checked.

As the analytical audit of the second law of thermodynamics is very complex, audits based on extreme cases have be done.

The first one consists of a comparison of the stress response between the newly formulated material model with an infinite friction coefficient and the *Onera Damage Model MicroStructure* (ODM_MS). Because of the hypothesis of infinite friction for the formulation of the ODM_MS, the stress responses of both models have to be equivalent. The displacement which is imposed to a shell element is the same as the one which was presented Fig. 2. The results in case of infinite friction are compared Fig. 6 and are entirely similar.

Rather, the second check consists of a comparison of the stress response between the newly formulated material model with an infinite friction coefficient and with an absence of friction at crack lips. The continuity of the shear stress response is preserved. The only difference concerns the shear stress evolution when the cracks are closed. The transmitted shear now corresponds to the stress which is transmitted by an healthy area of the material. As a consequence, the shear stress is smaller than in the case of infinite friction (Fig. 7).

The last check concerns the dissipated energy during crack lips displacements. This dissipated energy is represented graphically by hysteresis loop. Due to the clockwise orientation of these loops during friction mechanisms, and due to the symmetric behaviour of the friction mechanisms for positive or negative shear loading (which leads to recover the same stress state after an unloading/loading cycle), the dissipated energy is always positive. The second law of thermodynamics is thus ensured.

It is essential to note that very complex simulations (bulge tests,

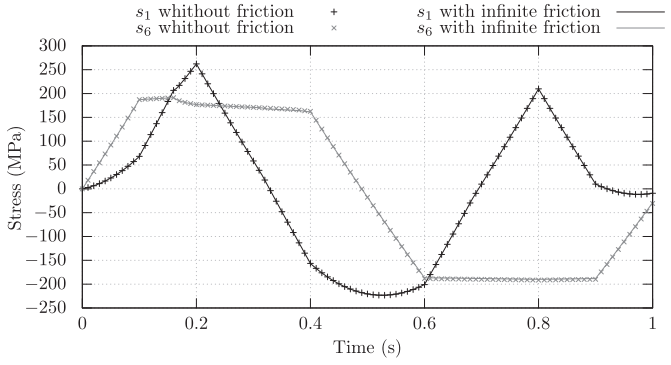

Fig. 6. Visualisation of the stored strain effect on the continuity of the stress response.

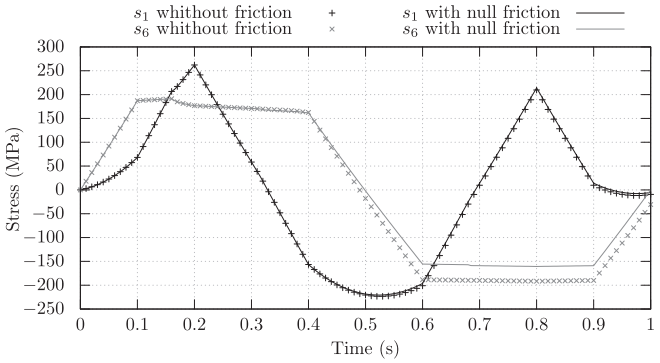

Fig. 7. Visualisation of the stored strain effect on the continuity of the stress response.

bending) have been carried out with the whole material model (viscoelasticity, fibre failure, delamination) and the second law of thermodynamics has always been verified.

3. Implementation

The aim of the implementation of a material model in a finite element software is to provide, at the current time step, the stress at an integration point according to the strain value given by the element formulation. It is carried out by the implementation of the developed constitutive model in an incremental loop.

In an explicit scheme, the computation time is conditioned by the efficiency of the material model. It is thus essential to limit as much as possible the internal loops. By using a strain-space formulation, the explicit scheme (stress obtained from the strain without iteration) is maintained. Thanks to the strain field provided by the finite element software in the material coordinate system, the thermodynamic forces are determined, leading to the damage evaluation. The crack closure indexes are evaluated and then the residual and the stored strains are computed by means of an incremental scheme. Note that the total Lagrangian framework helps to maintain the model efficiency by avoiding the use of complex algorithm to ensure the objectivity. Once the damage values, the crack closure indexes, the residual and the stored strains are determined, it is possible to calculate the stress thanks to the constitutive relation. The details are given in Algorithm 1.

Algorithm 1. Stress update algorithm with the matrix damage evaluation

Step 1 Calculation of the effective strain $\overrightarrow{e}^{+}$ (Equation (26)).
Step 2 Calculation of the thermodynamic forces y_i^{x} (Equations (25) and (50)).
Step 3 Calculation of the damage d_i^{m} (Equation (28)).
Step 4 Calculation of the crack closure index η_i^{m} (Equation (20)).
Step 5 Calculation of the effective stiffness tensor $\underline{\tilde{\mathbf{C}}}$ (Equation (19)).
Step 6 Calculation of the residual strain $\overrightarrow{e}^{\mathrm{r}}$ by following the iterative relation:

$$\overrightarrow{e}^{\mathrm{r}}_{t+\Delta t} = \overrightarrow{e}^{\mathrm{r}}_{t} + \underline{\mathbf{S}}^{0} \cdot \left(\sum_i \zeta_i \eta_i^{\mathrm{m}} \Delta d_i^{\mathrm{m}} \underline{\tilde{\mathbf{C}}} \cdot \underline{\mathbf{H}}_i^{\mathrm{m}} \cdot \underline{\tilde{\mathbf{C}}} \right) \cdot \frac{1}{2} \left(\overrightarrow{e}_{t+\Delta t} + \overrightarrow{e}_{t} \right).$$

Step 7 Calculation of the stored strain $\overrightarrow{e}^{\mathrm{s}}$ due to crack closure by following the iterative relation:

$$\overrightarrow{e}^{\mathrm{s}}_{t+\Delta t} = \overrightarrow{e}^{\mathrm{s}}_{t} - \underline{\mathbf{S}}^{0} \cdot \left(\sum_i \Delta \eta_i^{\mathrm{m}} d_i^{\mathrm{m}} \underline{\tilde{\mathbf{C}}} \cdot \underline{\mathbf{H}}_i^{\mathrm{m}} \cdot \underline{\tilde{\mathbf{C}}} \right) \cdot \frac{1}{2} \left(\overrightarrow{e}_{t+\Delta t} + \overrightarrow{e}_{t} \right).$$

Step 8 Calculation of the stored strain evolution due to friction mechanisms $\Delta \overrightarrow{e}_i^{\mathrm{s,tm}}$ (Equations in Section 2.8) and addition to the previously computed stored strain.
Step 9 Calculation of the stress $\overrightarrow{s}$ (Equation (14)).

The model is implemented for both solid or shell elements. For the shell elements, it is possible to use this model under plane stress assumption. It uses the three-dimensional formulation described in this work and a stress return algorithm to evaluate the thickness reduction. Another possibility is to use a two-dimensional formulation (without consideration of the out-of-plane strain and stress) but with the possibility to take into account the transverse shear behaviour of the material.

4. Identification

The parameter identification of the matrix damage model is done by means of two different experimental tests carried out independently on the different preforms. These tests are closed to the standardised monotonic tensile and in-plane shear tests, respectively the NF EN ISO 527-4 and NF EN ISO 14129 tests, in order to be easily reproducible in an industrial framework. The approach consists in eliminating gradually and systematically the unknown parameters.

These tests are carried out at room temperature on an electromagnetic device (Sintech 20D) which ensures 100 kN for the maximal load capacity and at a speed of 2 mm min^{-1}. The specimens are cut using the water-jet technique and their shape and dimensions, identical for both tests, are shown in Fig. 8. For technical reasons, aluminium heels with 1 mm thickness are used.

4.1. Longitudinal and transverse tensile tests

As a first step, the parameters describing the longitudinal and the transverse behaviours are determined through tensile tests in the fibre directions (Fig. 9). Some materials, like the ones taken as example, show an elastic brittle behaviour for longitudinal and transverse loading. In this case, the standardised NF EN ISO 527-4 test is used as such. Otherwise, in case of matrix cracks appearing before the final fracture of the coupon (due to the fibre failure), the tensile loading is increased on a cyclical basis. This last method allows to quantify the damage evolution and its effect on the mechanical behaviour.

Due to small strains at failure and none apparent damage, two gauges have been used to measure:

- $\varepsilon_{xx} = \varepsilon(\overrightarrow{X})$ the elongation in the centre of the coupon according to the $\overrightarrow{X}$ direction,
- $\varepsilon_{yy} = \varepsilon(\overrightarrow{Y})$ the elongation in the centre of the coupon according to the $\overrightarrow{Y}$ direction.

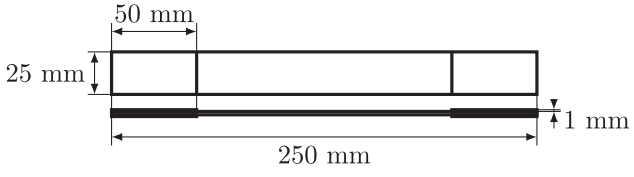

Fig. 8. Tensile and in-plane shear specimen geometry.

(a) Longitudinal tensile test.

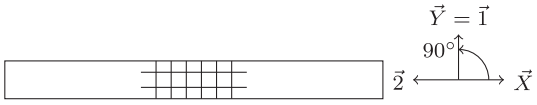

(b) Transverse tensile test.

Fig. 9. Material coordinate system $(\vec{1}, \vec{2})$ according to the specimen coordinate system $(\vec{X}, \vec{Y})$ for tensile tests.

The force applied to the coupon $F = \vec{F} \cdot \vec{X}$ is measured with a 100 kN load cell and then the engineering stress is obtained by:

$$\sigma_{xx} = \frac{F}{S^0} \tag{53}$$

where S^0 is the initial cross-section of the coupon.

The parameters E_1^0, α_1, E_2^0 and α_2 are then obtained through linear regressions of the curves $\frac{\sigma_{xx}}{\varepsilon_{xx}} = f(\varepsilon_{xx})$ from the longitudinal and transverse tensile tests, whereas ν_{12}^0 is obtained through the curve $-\frac{\varepsilon_{yy}}{\varepsilon_{xx}} = f(\varepsilon_{xx})$ from the longitudinal tensile test.

4.2. In-plane shear tests

Once the properties in the longitudinal and transverse directions are determined, the in-plane shear properties are obtained from a close version of the standardised NF EN ISO 14129 in-plane shear test. It consists of a tensile test according to an angle of 45° against the fibre directions (Fig. 10).

In this configuration, the matrix damage is important and leads to substantial non-linearity in the mechanical behaviour. Therefore, to quantify the level of damage and its effects on the behaviour, the tensile loading is increased on a cyclical basis.

Due to the large shear strain ability of the fabric preforms, extensometers are preferred to measure:

- ΔL_{xx} the relative displacement of both clips, initially set L_{xx}^0 apart, of the longitudinal extensometer,
- ΔL_{yy} the relative displacement of both clips, initially set L_{yy}^0 apart, of the transverse extensometer.

The in-plane shear angle is then given by:

$$\gamma_{12} = \frac{\Delta L_{xx}}{L_{xx}^0} - \frac{\Delta L_{yy}}{L_{yy}^0}. \tag{54}$$

The force applied to the coupon $F = \vec{F} \cdot \vec{X}$ is measured with a 40 kN load cell and then the engineering in-plane shear stress is obtained by:

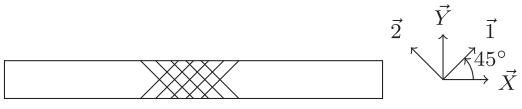

Fig. 10. Material coordinate system $(\vec{1}, \vec{2})$ according to the specimen coordinate system $(\vec{X}, \vec{Y})$ for in-plane shear tests.

$$\sigma_{12} = \frac{F}{2 \times S^0} \tag{55}$$

where S^0 is the initial cross-section of the coupon.

The initial slope of the curve $\sigma_{12} = f(\gamma_{12})$ defines the initial in-plane shear stiffness G_{12}^0. Then the identification of the parameters associated to the in-plane matrix damage is much more difficult due to the various coefficients which define the cumulative distribution functions of Weibull (Equation (28)), but also due to the interdependence between the damage and the friction mechanisms. Consequently, these parameters are obtained through an optimisation study to minimise the Mean Square Error (MSE) between the experimental and the numerical responses $F = f(\Delta L_{xx})$.

In the particular case of FRP made up with textile preforms two optimisation studies are needed due to the important out-of plane damage after the shear locking. The shear locking angle and the resulting Green-Lagrange shear strain at shear locking can be determined through the direct observation of the force-displacement curve. At shear locking, the material becomes significantly more rigid and a slight re-hardening appears. Once the shear angle determined, the same optimisation procedure as explained above is used on the responses before the shear locking in order to describe the in-plane damage evolution (d_1^m and d_2^m). Then an additional optimisation study is done on the out-of-plane damage evolution (d_3^m) and the parameter g_{12}^l describing the non-linearity of the in-plane shear stiffness due to shear locking.

The out-of-plane damage induced by matrix torsion between both transverse yarns is considered to occur after the shear locking. It can be understood by the study of the unit-cell deformation of a textile preform. By means of Digital Image Correlation carried out during in-plane shear tests, the rotation of the yarns have been observed (Fig. 11). The yarns start to rotate in the inter-yarn area. As soon as adjacent yarns come into contact (shear locking), the yarns start to rotate between them. This second mechanism leads to the torsion of the matrix between both transverse yarns, and consequently to the out-of-plane damage.

By proceeding in this manner, step by step on simple experimental tests, the global singularity of the solution is preserved and the parameters maintain a physical relevance. Moreover in case of balanced fabrics, the number of parameters is considerably lowered.

The results of the parameter identification are shown in Table 1.

5. Validation of the identification procedure

The present matrix damage model is implemented in FORTRAN 90 in a user material subroutine for the explicit finite element code LS-DYNA®, the whole model being dedicated to impact analysis and it requires an explicit finite element solver. In this validation procedure, shell elements are used with the two-dimensional formulation of the material model. Only a 20 mm long area in the middle of the experimental coupons is modelled. In this area the macroscopic homogeneity of the strain field has been verified by means of digital image correlation, which leads to a mesh convergence with only one shell element. Note that symmetric boundary conditions were used on the single shell element model. As a compromise between accuracy and efficiency, ten families of friction criterion have been used in this study.

This section presents the results of the identification procedure which have been presented Section 4 on three various fabric preforms, namely a bi-axial non-crimp fabric (see Fig. 1a), a 3K plain-weave woven (see Fig. 1b) and a 12K plain-weave woven. The optimisation procedures were carried out thanks to the commercial software LS-OPT® to minimise the Mean Square Error between the

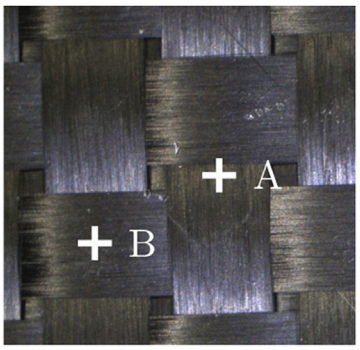

(a) Plain-weave woven unit-cell with Zones Of Interest.

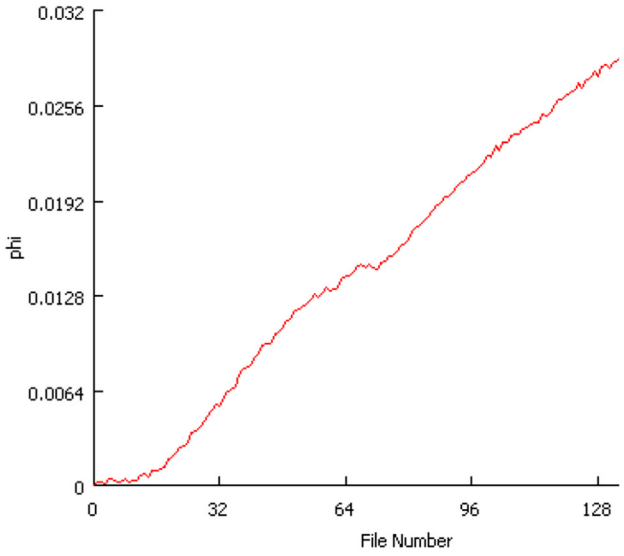

(b) Local rotation of the A-point.

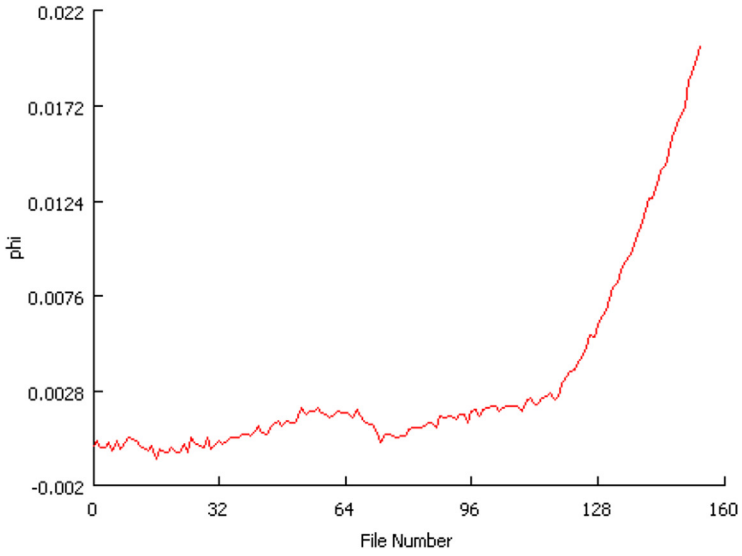

(c) Local rotation of the B-point

Fig. 11. Local rotations of the preforms obtained through Digital Image Correlation observation during in-plane shear tests.

numerical and the experimental responses. The sampling on the parameter range is done by using a D-Optimal method and the optimisation algorithm which has been used is the Adaptive Simulated Annealing.

As a first step of the validation, a longitudinal tensile test of both preforms is simulated and the results are compared with the experimental tests. Because of limited non-linearity for loading in the fibre directions, the mechanical behaviour is well described.

The in-plane shear behaviour, observed thanks to tensile tests with an angle of 45° according to the longitudinal fibre direction, is quite a bit more challenging to model. Although various fabric plies were tested, the matrix damage model is able to well describe their large non-linear behaviour as shown Figs. 12–14.

With few additional parameters compared to the previous formulations of the Onera Damage Model, because of the dependence between the friction mechanisms and the matrix crack density, the dissipated energy due to the hysteresis cycles can be assessed. Moreover, in case of positive/negative cyclic shearing this formulation avoids the previous limitations due to the hypothesis of infinite friction or null friction for the lips of the matrix cracks.

Finally, the use of the finite strain framework as well as the modelling of the shear locking phenomenon let to maintain the objectivity and the consideration of the real material orientation.

6. Concluding remarks on the matrix damage

The matrix damage model for fabric reinforced polymers is a close version of the Onera Damage MicroStructure model. A new evolution law for the stored strains has been presented. The friction mechanisms induced by the matrix cracks are now taken into account in a simple manner. It allows a good description of the shear behaviour, including the approximation of the dissipated energy due to the subsequent hysteresis loops.

Because of the large rotation of the yarns for shear loading, the model is extended in finite strain. The total Lagrangian formulation is used in order to well track the fibre orientation and ensure the objectivity. The shear locking is also introduced for the textile composites.

The procedure for the parameter identification is also provided. It consists of eliminating gradually and systematically the unknown parameters. It is done either by direct measurement on the experimental results, or by optimisation of restrained sets of parameters in order to keep the singularity and the physical meaning of the results.

From the numerical point of view, the model is implemented in the commercial finite element software LS-DYNA®. It is validated through standardised tensile and in-plane shear experimental

Table 1
Parameters for the intralaminar matrix damage model for the various fabric preforms.

Parameters	Units	NCF	3K woven	12K woven
$E_1^0 = E_2^0$	MPa	55,562	46,589	49,212
$\alpha_1 = \alpha_2$	MPa	277,722	147,722	286,678
ν_{21}	/	0.13	0.10	0.05
G_{12}^0	MPa	3000	4910	3236
g_{12}^{I}	MPa	0	2100	0
e_6^{I}	/	0	0.17	0
$b_1 = b_2$	/	0	0	0
$d_{c(1)}^{\mathrm{nm}} = d_{c(2)}^{\mathrm{nm}}$	/	0	0	0
$y_{0(1)}^{\mathrm{nm}} = y_{0(2)}^{\mathrm{nm}}$	/	0	0	0
$y_{c(1)}^{\mathrm{nm}} = y_{c(2)}^{\mathrm{nm}}$	/	0	0	0
$p_1^{\mathrm{nm}} = p_2^{\mathrm{nm}}$	/	0	0	0
$d_{c(1)}^{\mathrm{tm}} = d_{c(2)}^{\mathrm{tm}}$	/	0.6324	0.6745	0.6992
$y_{0(1)}^{\mathrm{tm}} = y_{0(2)}^{\mathrm{tm}}$	/	0.0041	0.0041	0.0041
$y_{c(1)}^{\mathrm{tm}} = y_{c(2)}^{\mathrm{tm}}$	/	2.124	1.729	0.04371
$p_1^{\mathrm{tm}} = p_2^{\mathrm{tm}}$	/	0.2248	0.097	0.281
$d_{c(3)}^{\mathrm{tm}}$	/	/	0	/
$y_{0(3)}^{\mathrm{tm}}$	/	/	0	/
$y_{c(3)}^{\mathrm{tm}}$	/	/	0	/
p_3^{tm}	/	/	0	/
$h_{m(1)}^{\mathrm{I}} = h_{m(2)}^{\mathrm{I}}$	/	0	0	0
$h_{m(1)}^{\mathrm{II}} = h_{m(2)}^{\mathrm{II}}$	/	1	1	1.0467
$h_{m(1)}^{\mathrm{III}} = h_{m(2)}^{\mathrm{III}}$	/	0	0	0
$d_{c(3)}^{\mathrm{p}}$	/	/	0.3253	/
$y_{0(3)}^{\mathrm{p}}$	/	/	17.9	/
$y_{c(3)}^{\mathrm{p}}$	/	/	20	/
p_3^{p}	/	/	1.751	/
$h_{m(3)}^{\mathrm{p}}$	/	/	1	/
$\zeta_1 = \zeta_2$	/	0	0	0.011
ζ_3	/	/	0	/
$m_1^0 = m_2^0$	/	0.00838	0.0498	0.00558
$m_1^m = m_2^m$	/	12.48	4	7.914
m_3^0	/	/	0.3	/
m_3^m	/	/	179.5	/
$e_1^0 = e_2^0$	/	0.01	0.01	0.01
$a_1^{\mathrm{m}} = a_2^{\mathrm{m}}$	/	0	0	0
e_3^0	/	0.01	0.01	0.01

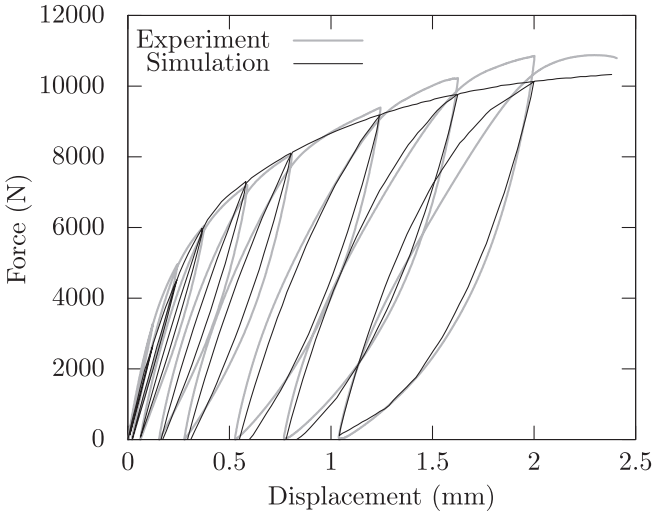

Fig. 12. Reaction force comparisons between the numerical model and the experimental data for in-plane shear tests of the bi-axial non-crimp fabric.

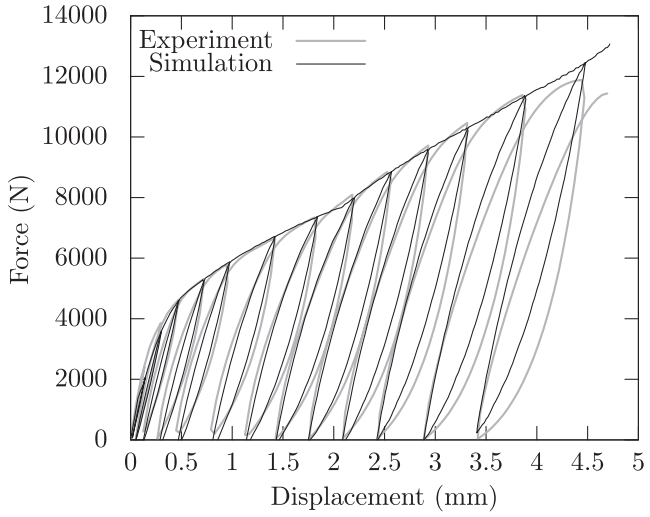

Fig. 13. Reaction force comparisons between the numerical model and the experimental data for in-plane shear tests of the 3K plain weave woven fabric.

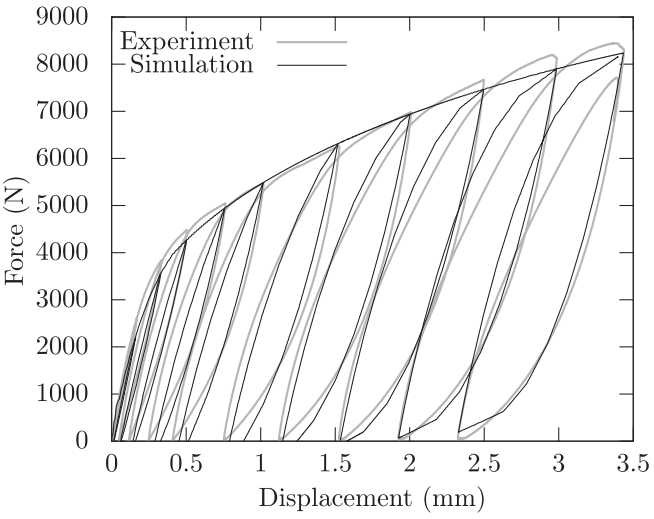

Fig. 14. Reaction force comparisons between the numerical model and the experimental data for in-plane shear tests of the 12K plain weave woven fabric.

tests. The simulation results show the good efficiency of the proposed model for fully different fabric preforms, such as non-crimp or woven.

However, in order to fully simulate the behaviour of layered fabric composites, additional physical phenomena have to be taken into account. Such is the case, for instance, viscoelasticity, fibre failure or intralaminar damage. The newly introduced friction mechanisms are also as simple as possible (based on Coulomb criterion) and could be further improved.

Acknowledgments

The present research work has been supported by International Campus on Safety and Intermodality in Transportation, the Region Nord Pas de Calais, the European Community, the Delegation Regionale a la Recherche et a la Technologie, the gs5:Ministère de l'Enseignement Supérieur et de la Recherche, the Centre National de la Recherche Scientifique and TOYOTA MOTOR EUROPE: the authors gratefully acknowledge the support of these institutions.

References

[1] Abisset E, Daghia F, Ladevèze P. On the validation of a damage mesomodel for laminated composites by means of open-hole tensile tests on quasi-isotropic laminates. Compos Part A Appl Sci Manuf Oct. 2011;42(10):1515–24. http://www.sciencedirect.com/science/article/pii/S1359835X11002107.

[2] Aiello G. Utilisation des composites à matrice céramique sic/sic comme matériau de structure de composants internes du tore d'un réacteur à fusion [Ph.D. thesis]. 2001.

[3] Allix O, Feissel P, Thévenet P. A delay damage mesomodel of laminates under dynamic loading: basic aspects and identification issues. Comput Struct 2003;81(12):1177–91. http://www.sciencedirect.com/science/article/pii/S004579490300035X.

[4] Allix O, Ladevèze P. Interlaminar interface modelling for the prediction of delamination. Compos Struct 1992;22(4):235–42. http://www.sciencedirect.com/science/article/pii/026382239290060P.

[5] Andrieux S, Bamberger Y, Marigo J-J. Un modèle de matériau microfissuré pour les bétons et les roches. J Mécan Thor Appl 1986;5(3):471–513. http://cat.inist.fr/?aModele=afficheN&cpsidt=8203892.

[6] Apuzzo A, Barretta R, Luciano R. Some analytical solutions of functionally graded Kirchhoff plates. Compos Part B Eng Jan. 2015;68:266–9. http://www.sciencedirect.com/science/article/pii/S1359836814003862.

[7] Balieu R. Modèle viscoélastique-viscoplastique couplé avec endommagement pour les matériaux polymères semi-cristallins [Ph.D. thesis]. Université de Valenciennes et du Hainaut-Cambresis; 2012.

[8] Barretta R, Feo L, Luciano R, Marotti de Sciarra F. Variational formulations for functionally graded nonlocal Bernoulli-Euler nanobeams. Compos Struct Oct. 2015;129:80–9. http://www.sciencedirect.com/science/article/pii/S0263822315002068.

[9] Barretta R, Luciano R. Exact solutions of isotropic viscoelastic functionally graded Kirchhoff plates. Compos Struct 2014;118:448–54. http://www.sciencedirect.com/science/article/pii/S0263822314003675.

[10] Barretta R, Luciano R. Analogies between Kirchhoff plates and functionally graded Saint-Venant beams under torsion. Contin Mech Thermodyn May 2015;27(3):499–505. http://link.springer.com/article/10.1007/s00161-014-0385-2.

[11] Barretta R, Luciano R, Willis JR. On torsion of random composite beams. Compos Struct Nov. 2015;132:915–22. http://www.sciencedirect.com/science/article/pii/S0263822315005334.

[12] Basista M, Gross D. The sliding crack model of brittle deformation: an internal variable approach. Int J Solids Struct 1998;35(5):487–509. http://www.sciencedirect.com/science/article/pii/S0020768397000310.

[13] Berthe J. Comportement thermo-visco-élastique des composites cmo - de la statique à la dynamique grande vitesse [Ph.D. thesis]. Ecole Centrale de Lille; 2013.

[14] Bonet J, Burton AJ. A simple orthotropic, transversely isotropic hyperelastic constitutive equation for large strain computations. Comput Methods Appl Mech Eng 1998;162(1–4):151–64. http://www.sciencedirect.com/science/article/pii/S0045782597003393.

[15] Bouvet C, Rivallant S, Barrau JJ. Low velocity impact modeling in composite laminates capturing permanent indentation. Compos Sci Technol Nov. 2012;72(16):1977–88. http://www.sciencedirect.com/science/article/pii/S0266353812003223.

[16] Camanho P, Bessa M, Catalanotti G, Vogler M, Rolfes R. Modeling the inelastic deformation and fracture of polymer composites. Part II. Smeared crack model. Mech Mater 2013;59:36–49. http://www.sciencedirect.com/science/article/pii/S0167663612002128.

[17] Cervera M, Chiumenti M. Smeared crack approach: back to the original track. Int J Numer Anal Methods Geomech Oct. 2006;30(12):1173–99. http://onlinelibrary.wiley.com/doi/10.1002/nag.518/abstract.

[18] Chaboche JL. Anisotropic creep damage in the framework of continuum damage mechanics. Nucl Eng Des 1984;79(3):309–19. http://www.sciencedirect.com/science/article/pii/0029549384900463.

[19] Chaboche J-L. Damage induced anisotropy: on the difficulties associated with the active/passive unilateral condition. Int J Damage Mech Apr. 1992;1(2):148–71. http://ijd.sagepub.com/content/1/2/148.

[20] Chaboche J-L. Development of continuum damage mechanics for elastic solids sustaining anisotropic and unilateral damage. Int J Damage Mech Oct. 1993;2(4):311–29. http://ijd.sagepub.com/content/2/4/311.

[21] Chaboche J-L, Maire J-F. A new micromechanics based CDM model and its application to CMC's. Aerosp Sci Technol 2002;6(2):131–45. http://www.sciencedirect.com/science/article/pii/S1270963802011549.

[22] Charmetant A, Orliac J, Vidal-Sallé E, Boisse P. Hyperelastic model for large deformation analyses of 3d interlock composite preforms. Compos Sci Technol Jul. 2012;72(12):1352–60. http://linkinghub.elsevier.com/retrieve/pii/S0266353812001790.

[23] Cho M, Kim J-S. Higher-order zig-zag theory for laminated composites with multiple delaminations. J Appl Mech Oct. 2000;68(6):869–77. http://dx.doi.org/10.1115/1.1406959.

[24] Cousigné O, Moncayo D, Coutellier D, Camanho P, Naceur H. Numerical modeling of nonlinearity, plasticity and damage in CFRP-woven composites for crash simulations. Compos Struct 2014;115:75–88. http://www.sciencedirect.com/science/article/pii/S0263822314001846.

[25] Daniel I, Werner B, Fenner J. Strain-rate-dependent failure criteria for composites. Compos Sci Technol 2011;71(3):357–64. http://www.sciencedirect.com/science/article/pii/S0266353810004677.

[26] Gambarotta L, Lagomarsino S. A microcrack damage model for brittle materials. Int J Solids Struct Jan. 1993;30(2):177–98. http://www.sciencedirect.com/science/article/pii/002076839390059G.

[27] Greve L, Pickett AK. Delamination testing and modelling for composite crash simulation. Compos Sci Technol 2006;66(6):816–26. http://www.sciencedirect.com/science/article/pii/S0266353804003549.

[28] Halm D, Dragon A. An anisotropic model of damage and frictional sliding for brittle materials. Eur J Mech - A/Solids 1998;17(3):439–60. http://www.sciencedirect.com/science/article/pii/S0997753898800545.

[29] Heil C, Cardon A, Brinson H. The nonlinear viscoelastic response of resin matrix composite laminates. Tech. rep. DTIC Document; 1984.

[30] Hill R. A theory of the yielding and plastic flow of anisotropic metals. Proc Roy Soc Lond Ser A Math Phys Sci 1948;193(1033):281–97. http://www.jstor.org/stable/97993.

[31] Holzapfel GA, Gasser TC. A viscoelastic model for fiber-reinforced composites at finite strains: continuum basis, computational aspects and applications. Comput Methods Appl Mech Eng 2001;190(34):4379–403. http://www.sciencedirect.com/science/article/pii/S0045782500003236.

[32] Huchette C, Lévêque D, Carrère N. A multiscale damage model for composite laminate based on numerical and experimental complementary tests. In: IUTAM symposium on multiscale modelling of damage and fracture processes in composite materials. Springer; 2006. p. 241–8.

[33] Jirásek M, Rolshoven S. Comparison of integral-type nonlocal plasticity models for strain-softening materials. Int J Eng Sci 2003;41(13–14):1553–602. http://www.sciencedirect.com/science/article/pii/S0020722503000272.

[34] Johnson A, Pickett A, Rozycki P. Computational methods for predicting impact damage in composite structures. Compos Sci Technol Nov. 2001;61(15):2183–92. http://www.sciencedirect.com/science/article/pii/S0266353801001117.

[35] Kachanov LM. Time of the rupture process under creep conditions. Izv Akad Nauk S.S.R Otd Tech Nauk 1958;8:26–31.

[36] Kachanov ML. A microcrack model of rock inelasticity. Part I. Frictional sliding on microcracks. Mech Mater Jan. 1982;1(1):19–27. http://www.sciencedirect.com/science/article/pii/0167663682900217.

[37] Key CT, Schumacher SC, Hansen AC. Progressive failure modeling of woven fabric composite materials using multicontinuum theory. Compos Part B Eng Mar. 2007;38(2):247–57. http://www.sciencedirect.com/science/article/pii/S1359836806000552.

[38] Khandan R, Noroozi S, Sewell P, Vinney J. The development of laminated composite plate theories: a review. J Mater Sci Feb. 2012;47(16):5901–10. http://link.springer.com/article/10.1007/s10853-012-6329-y.

[39] Kim J-S, Oh J, Cho M. Efficient analysis of laminated composite and sandwich plates with interfacial imperfections. Compos Part B Eng 2011;42(5):1066–75. http://www.sciencedirect.com/science/article/pii/S135983681100117X.

[40] Kimura H, Kubomura K. Mechanical properties and applications of pitch-based carbon fiber reinforced plastics (CFRP). Nippon Steel Technical Report; 1993. 59(0), http://www.nssmc.com/en/tech/report/nsc/pdf/5912.pdf.

[41] Krajcinovic D, Fanella D. A micromechanical damage model for concrete. Eng Fract Mech Jan. 1986;25(5):585–96. http://www.sciencedirect.com/science/article/pii/001379448690024X.

[42] Ladeveze P. A damage computational approach for composites: basic aspects and micromechanical relations. Comput Mech Dec. 1995;17(1–2):142–50. http://link.springer.com/article/10.1007/BF00356486.

[43] Ladeveze P, LeDantec E. Damage modelling of the elementary ply for laminated composites. Compos Sci Technol 1992;43(3):257–67. http://www.sciencedirect.com/science/article/pii/026635389290097M.

[44] Ladevèze P, Lubineau G. On a damage mesomodel for laminates: micro-meso relationships, possibilities and limits. Compos Sci Technol Nov. 2001;61(15):2149–58. http://www.sciencedirect.com/science/article/pii/S0266353801001099.

[45] Ladevéze P, Lubineau G, Marsal D. Towards a bridge between the micro- and mesomechanics of delamination for laminated composites. Compos Sci Technol 2006;66(6):698–712. http://www.sciencedirect.com/science/article/pii/S0266353804003665.

[46] Lemaitre J. Evaluation of dissipation and damage in metals submitted to dynamic loading. Mech Behav Mater 1972:540–9.

[47] Lo KH, Christensen RM, Wu EM. A high-order theory of plate deformation. Part 2. Laminated plates. J Appl Mech 1977;44(4):669–76. http://dx.doi.org/10.1115/1.3424155.

[48] Long S, Yao X, Zhang X. Delamination prediction in composite laminates under low-velocity impact. Compos Struct Nov. 2015;132:290–8. http://www.sciencedirect.com/science/article/pii/S026382231500402X.

[49] Lou Y, Schapery RA. Viscoelastic behavior of a nonlinear fiber-reinforced plastic. Tech. rep. DTIC Document; 1970.

[50] Maimí P, Camanho PP, Mayugo JA, Turon A. Matrix cracking and delamination in laminated composites. Part I. Ply constitutive law, first ply failure and onset of delamination. Mech Mater 2011;43(4):169–85. http://www.sciencedirect.com/science/article/pii/S0167663610001663.

[51] Mallikarachchi H, Pellegrino S. Failure criterion for two-ply plain-weave CFRP laminates. J Compos Mater Sep.2012;47(11):1357–75. http://jcm.sagepub.com/content/early/2012/09/23/0021998312447208.

[52] Marcin L. Modélisation du comportement, de l'endommagement et de la rupture de matériaux composites á renforts tissés pour le dimensionnement robuste de structures [Ph.D. thesis]. Université Bordeaux 1; 2010. http://tel.archives-ouvertes.fr/tel-00481601/.
[53] May M. Numerical evaluation of cohesive zone models for modeling impact induced delamination in composite materials. Compos Struct 2015;133:16–21. http://www.sciencedirect.com/science/article/pii/S0263822315005760.
[54] Peng X, Guo Z, Du T, Yu W-R. A simple anisotropic hyperelastic constitutive model for textile fabrics with application to forming simulation. Compos Part B Eng 2013;52(0):275–81. http://www.sciencedirect.com/science/article/pii/S1359836813001625.
[55] Pensée V, Kondo D, Dormieux L. Micromechanical analysis of anisotropic damage in brittle materials. J Eng Mech 2002;128(8):889–97. http://ascelibrary.org/doi/10.1061/%28ASCE%290733-9399%282002%29128%3A8%28889%29.
[56] Pijaudier-Cabot G, Bazant ZP. Nonlocal damage theory. J Eng Mech 1987;113(10):1512–33.
[57] Pinho ST, Dàvila CG, Camanho PP, Iannucci L, Robinson P. Failure models and criteria for FRP under in-plane or three-dimensional stress states including shear non-linearity. NASA Technical Memorandum 213530. 2005. p. 18.
[58] Pinho ST, Iannucci L, Robinson P. Formulation and implementation of decohesion elements in an explicit finite element code. Compos Part A Appl Sci Manuf 2006a;37(5):778–89. http://www.sciencedirect.com/science/article/pii/S1359835X05002691.
[59] Pinho ST, Iannucci L, Robinson P. Physically-based failure models and criteria for laminated fibre-reinforced composites with emphasis on fibre kinking. Part I. Development. Compos Part A Appl Sci Manuf 2006b;37(1):63–73. http://www.sciencedirect.com/science/article/pii/S1359835X05002198.
[60] Puck A, Schürmann H. Failure analysis of FRP laminates by means of physically based phenomenological models. Compos Sci Technol Sep. 2002;62(12–13):1633–62. http://www.sciencedirect.com/science/article/pii/S0266353801002081.
[61] Rabotnov YN. Creep rupture. In: Proc. XII, Int. Cong. Appl. Mech. Stanford: Springer; 1968.
[62] Raimondo L, Iannucci L, Robinson P, Curtis PT. Modelling of strain rate effects on matrix dominated elastic and failure properties of unidirectional fibre-reinforced polymer-matrix composites. Compos Sci Technol 2012;72(7):819–27. http://www.sciencedirect.com/science/article/pii/S026635381200070X.
[63] Reddy JN. A simple higher-order theory for laminated composite plates. J Appl Mech 1984;51(4):745–52. http://dx.doi.org/10.1115/1.3167719.
[64] Reddy JN. A generalization of two-dimensional theories of laminated composite plates. Commun Appl Numer Methods 1987;3(3):173–80. http://onlinelibrary.wiley.com/doi/10.1002/cnm.1630030303/abstract.
[65] Schieffer A. Modélisation multiéchelle du comportement thermo-mécanique des CMO et prise en compte des effets du vieillissement thermique [Ph.D. thesis]. Jan. 2003. http://www.theses.fr/2003TROY0002.
[66] Schieffer A, Maire J-F, Lévêque D. A coupled analysis of mechanical behaviour and ageing for polymer-matrix composites. Compos Sci Technol Mar. 2002;62(4):543–9. http://www.sciencedirect.com/science/article/pii/S0266353801001464.
[67] Sciuva MD, Icardi U. Analysis of thick multilayered anisotropic plates by a higher order plate element. AIAA J 1995;33(12):2435–7. http://dx.doi.org/10.2514/3.13009.
[68] Simo JC, Hughes TJ. Viscoelasticity. In: Computational inelasticity. No. 7 in Interdisciplinary applied mathematics. New York: Springer; 1998. p. 336–73. http://dx.doi.org/10.1007/0-387-22763-6_10. http://link.springer.com/chapter/10.1007/0-387-22763-6_10.
[69] Strömberg L, Ristinmaa M. FE-formulation of a nonlocal plasticity theory. Comput Methods Appl Mech Eng Sep. 1996;136(1–2):127–44. http://www.sciencedirect.com/science/article/pii/0045782596009978.
[70] Sumarac D, Krajcinovic D. A self-consistent model for microcrack-weakened solids. Mech Mater Mar. 1987;6(1):39–52. http://www.sciencedirect.com/science/article/pii/0167663687900214.
[71] Tsai SW, Wu EM. A general theory of strength for anisotropic materials. J Compos Mater Jan. 1971;5(1):58–80. http://jcm.sagepub.com/content/5/1/58.
[72] Tuttle ME, Brinson HF. Prediction of the long-term creep compliance of general composite laminates. Exp Mech Mar. 1986;26(1):89–102. http://link.springer.com/article/10.1007/BF02319961.
[73] Wrzesniak A, Dascalu C, Bésuelle P. A two-scale time-dependent model of damage: influence of micro-cracks friction. Eur J Mech - A/Solids Jan. 2015;49:345–61. http://www.sciencedirect.com/science/article/pii/S099775381400117X.
[74] Yeh H-Y, Kim CH. The Yeh-Stratton Criterion for composite materials. J Compos Mater May 1994;28(10):926–39. http://jcm.sagepub.com/content/28/10/926.
[75] Zaoutsos SP, Papanicolaou GC, Cardon AH. On the non-linear viscoelastic behaviour of polymer-matrix composites. Compos Sci Technol 1998;58(6):883–9. http://www.sciencedirect.com/science/article/pii/S0266353897001954.
[76] Zhu QZ, Kondo D, Shao JF. Micromechanical analysis of coupling between anisotropic damage and friction in quasi brittle materials: role of the homogenization scheme. Int J Solids Struct Mar. 2008;45(5):1385–405. http://www.sciencedirect.com/science/article/pii/S002076830700399X.